Case Studies in Engineering Failure Analysis 5–6 (2016) 1–9

Contents lists available at ScienceDirect

Case Studies in Engineering Failure Analysis

journal homepage: www.elsevier.com/locate/csefa

Effect analysis of an arc-strike-induced defect on the failure of a post-tensioned threadbar

Jesús Chao *, Carmen Peña

Mechanical Testing Laboratory, Centro Nacional de Investigaciones Metalúrgicas (CENIM-CSIC), Avda. Gregorio del Amo 8, 28040 Madrid, Spain

ARTICLE INFO

Article history:
Received 3 September 2015
Received in revised form 30 October 2015
Accepted 2 November 2015
Available online 10 November 2015

Keywords:
Prestressing threadbar
Arc strike
Perlitic steel
Surface cracks
Fracture toughness

ABSTRACT

A temporary threadbar used for precast segmental construction broke during the post-tensioning stage before reaching the service load. Failure analysis showed that the premature failure of the bar was due to the presence of an arc strike. The arc strike effects on the material and threadbar integrity are considered.

1. Introduction

Previous works have demonstrated that the mechanical properties of pre-stressed steel bars are sensitive to the presence of small (<1 mm) surface defects, such as scratches, cracks or pits, because of a limited material fracture toughness and a necessity to apply a high (0.7 times the ultimate tensile load) stress level [1,2].

This study analyzes the reason why a temporary threaded high-strength bar (UTS > 1000 MPa; Ø = 26.5 mm) used for precast segmental construction broke during the post-tensioning process before reaching 0.7 times the ultimate tensile load. Therefore, a complete characterization of the threadbar was performed, which included fractured bar failure analysis and fracture surface fractographic analysis. Based on the obtained information, a discussion of the results was undertaken.

2. Threadbar characterization

2.1. Chemical composition

The chemical composition of the threadbar, determined using glow discharge optical emission spectrometry (GDOES), is shown in Table 1. This chemical analysis verifies the compositional limits ($S < 0.05$, $P < 0.04$) specified in the ASTM A722 standard. Furthermore, this composition is in accordance with the chemical composition of UNS G10700 steel.

* Corresponding author.
E-mail address: jchao@cenim.csic.es (J. Chao).

http://dx.doi.org/10.1016/j.csefa.2015.11.001

Table 1
Chemical composition of the prestressing bar.

Element	C	Si	Mn	P	S	Cr	Ni	Mo	Cu
Weight %	0.67	0.28	0.85	0.011	0.014	0.026	0.011	<0.010	0.028

2.2. Microstructural analysis

Microstructural analysis was performed on a cross section far from the fracture, which was etched with 2% Nital. The microstructure was a fine perlite in the bar center and a tempered martensite on the surface ring that was approximately 1.4 mm deep, Fig. 1. These microstructure differences are caused by cooling rate differences from the rolling temperature to room temperature during bar processing.

2.3. Hardness tests

Because of the abovementioned microstructural differences, Vickers hardness (9.8 N) tests were performed along the cross section radius of the bar. No significant differences in hardness were found. The hardness value was 343 ± 19 ($n = 22$), the maximum value ($\approx$370 HV1) was located near the surface, and the minimum value of 286 HV1 was near the cross section center. No clear trend of the hardness with distance from the surface was observed.

2.4. Tensile tests

Two types of samples were tested: threadbar samples with a 700 mm length and tensile specimens with a 24.4 mm diameter and 150 mm gage length. This diameter was chosen to obtain from the threadbar cross section, the maximum circular cross section at the specimen gage length. Tensile tests of the threadbars were carried out according to ISO 15630-3 [3], whereas those of the specimen were carried out according to ISO 6892-1 [4]. Table 2 presents the pull test results. To obtain the YS and UTS of the threadbar, the nominal cross section (552 mm^2) was considered. The obtained results for both test types agree with each other and confirm the ASTM A722 standard specifications [5]. In both cases, the fracture occurred after an appreciable plastic deformation. Apparently, the fracture initiation modes are different, as shown in Fig. 2. In the tensile specimen, the fracture initiates at the cross section center, and in the threadbar, the fracture initiates at the surface. This can be explained by taking into account the fact that the ductile fracture initiates at the location where the stress triaxiality state is maximum. For the tensile specimen, the fracture initiates at the center of the cross section, which is the location where the stress triaxiality state is maximum (once the necking has developed) after, the fracture concentrically advanced via microvoid coalescence and finalized unsteadily via a cleavage mechanism with isolated ductile areas. For the threadbar, the fracture occurred similarly, except for the fracture initiation, which occurred at the surface ridge basis because this is the location where the stress triaxiality state is maximum. It is likely that small elongation differences were caused by these fracture initiation mode differences.

2.5. Fracture toughness tests

The single edge notch bend specimens with a 10 mm thickness, 10 mm width and 55 mm length were machined from the bar according to the ASTM E1820 standard [6]. The provisional fracture toughness K_Q values were found to be invalid for obtaining a K_{Ic} value according to the specifications in the abovementioned ASTM standard. Thus, the provisional J_Q values were calculated from the load versus load-line displacement curves according to the ASTM E1820 standard [6]. Because the J_Q values meet the size criteria of the standard, they qualify as J_c values. This implies that the obtained values are insensitive to the specimen dimensions. The fracture toughness K_{Jc} value was calculated from the J integral value at the onset of a brittle fracture J_c using the following expression:

$$K_{Jc} = \sqrt{\frac{J_c E}{1-\upsilon^2}} \tag{1}$$

where E is Young's modulus and υ is Poisson's ratio.

Thus, the valid values of the K_{Jc} fracture toughness were: 71.2–69.5–70.5 MPa $m^{1/2}$.

Fig. 3 shows a typical SEM image of the fracture mode of the specimens. It demonstrates the fatigue precrack, the stretching of the fatigue precrack-tip with some isolated microvoids and the final fracture via cleavage.

3. Failure analysis of the threadbar

The threadbar failure occurred without plastic deformation. When the fracture surface was observed with a naked eye, some directional tear ridges were observed (Fig. 4(a) and (b)). By tracing back the directional features it was possible to identify the fracture initiation zone. The fracture started from a linear segment with an approximate 9 mm length located

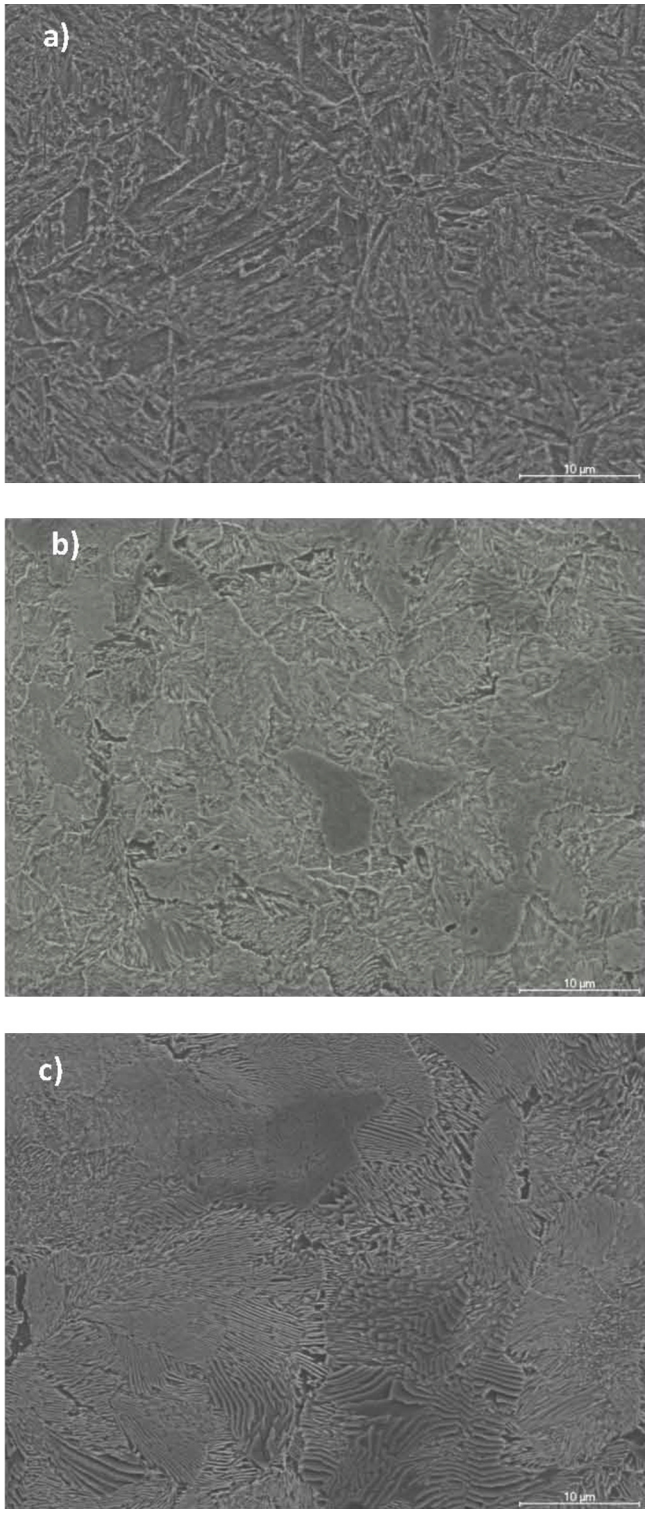

Fig. 1. SEM micrographs showing the threadbar microstructure far from the fracture. (a) Near the surface, the microstructure consists of tempered martensite. (b) At one-quarter of the diameter, the microstructure consists of bainite and fine perlite. (c) Near the bar center, the microstructure consists of perlite.

2.5 mm from the bar surface. By analyzing the bar surface in the immediate vicinity of the fracture initiation zone, a material alteration, presumably caused by an arc strike (AS), was observed (Fig. 4(c) and (d)).

An AS is a defect or material discontinuity, which is well defined in handbooks and welding standards. It results from unintentionally briefly initiating an arc on any metal [7,8]. This is usually attributed to electrodes or electrode holders

Table 2
Tensile properties of the prestressing bar.

Test	YS (MPa)	UTS (MPa)	A_u (%)	A_r (%)	RA (%)
Bar	1013	1125	6.1	10.6	–
Specimen	990	1128	8.9	12.8	38.7

contacting the workpiece, ground clamps being too close to the bar, bare spots in the welding cable or a combination of these [9]. The material alteration produced by an AS consists of a localized re-melted metal and a heat affected zone [8].

To demonstrate how the AS modified the threadbar material, a longitudinal cross section containing the fracture profile through the initiation zone was metallographically prepared, as shown in Fig. 4(b) and (d). The following was observed: a remnant of molten metal with a microstructure consisting of proeutectoid ferrite and ferrite side plates in prior austenitic grain boundaries and intracolumnar very fine perlite (Fig. 5(a)); a cracked white layer of approximately 1 mm thickness of unmelted material transformed by the heat to martensite with a profusion of defects in the grain boundaries (Fig. 5(b)). The fracture initiation took place at the interface between the molten metal, which was presumably lost during fracturing, and the martensite layer, as shown in Fig. 5(b) (left). Furthermore, the Vickers hardness (9.8 N) variation with distance from the surface at the AS vicinity was investigated. Fig. 6 reveals that the hardness increases from 350 HV1 in the unaffected material to 800 HV1 in the martensite layer. The hardness of the molten metal remnant was 388 ± 60 HV0.3 ($n = 5$).

To evaluate the AS-induced damage and its effects on the tensile behavior, various AS were deliberately caused in the laboratory via the instantaneous contact of an electrode or an electrode holder with bar samples of a 600 mm length that were previously attached to the grounding clamp. Each bar sample exhibited at least three AS that were randomly placed along the central zone of the bar. It is worth mentioning that similar peak values and distributions of the Vickers hardness to those of the broken service bar were obtained.

The AS longitudinal and transverse cross sections were prepared metallographically to evaluate the AS-induced damage. Fig. 7 shows representative AS-induced defects found in the bars. Only in one AS were no defects observed (Fig. 7(a)). In other cases, cracks at the molten metal parallel to the bar axis (Fig. 7(b)), at the heat-affected zone bordering the molten metal (Fig. 7(c)) or a small surface crack emerging at the toe of the molten metal and contouring it (Fig. 7(d)) were found. Because of

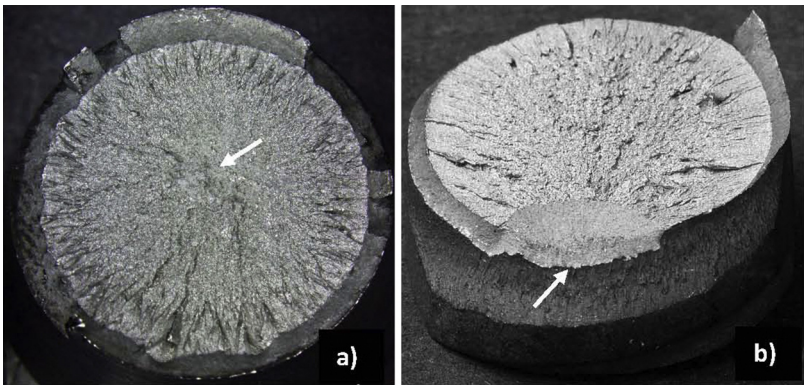

Fig. 2. Appearance of fractures in the tensile specimens: (a) Machined tensile specimen. (b) Threaded bar sample. The white arrows indicate the initiation point of the fracture.

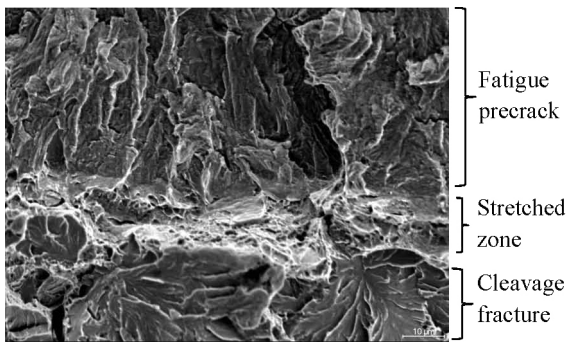

Fig. 3. SEM micrograph showing the fracture surface fractographic features of the fracture toughness specimens.

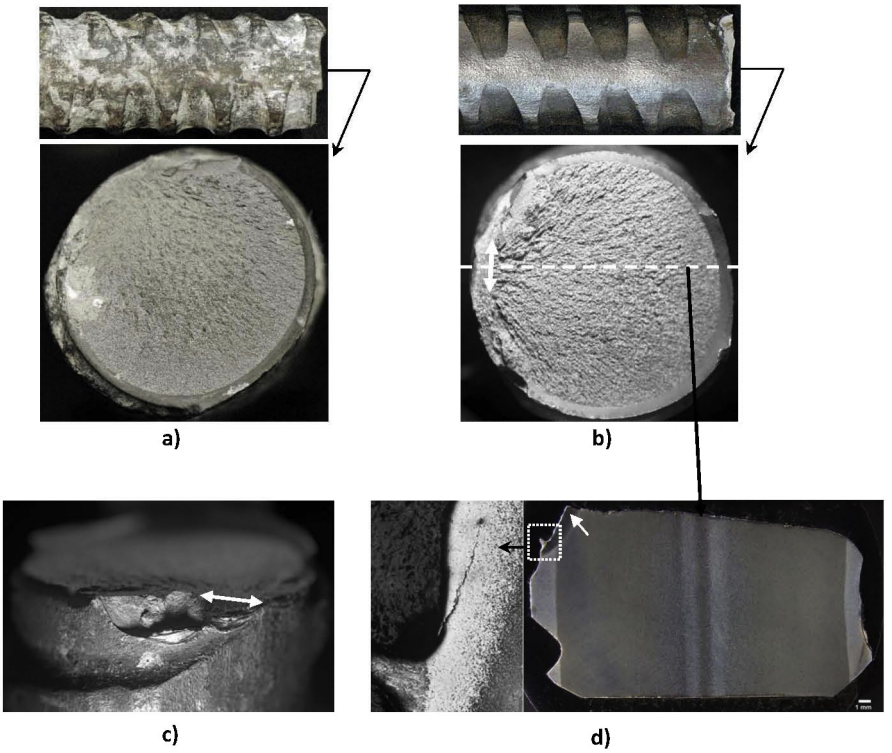

Fig. 4. Macroscopic aspects of the threadbar broken during service: (a) as received state. (b) After the cleaning process. The double white arrow indicates the linear segment from which the fractures initiated. (c) View of the surface affected by the AS. (d) The longitudinal cross section showing the AS-induced material alteration; the white arrow indicates the fracture initiation point.

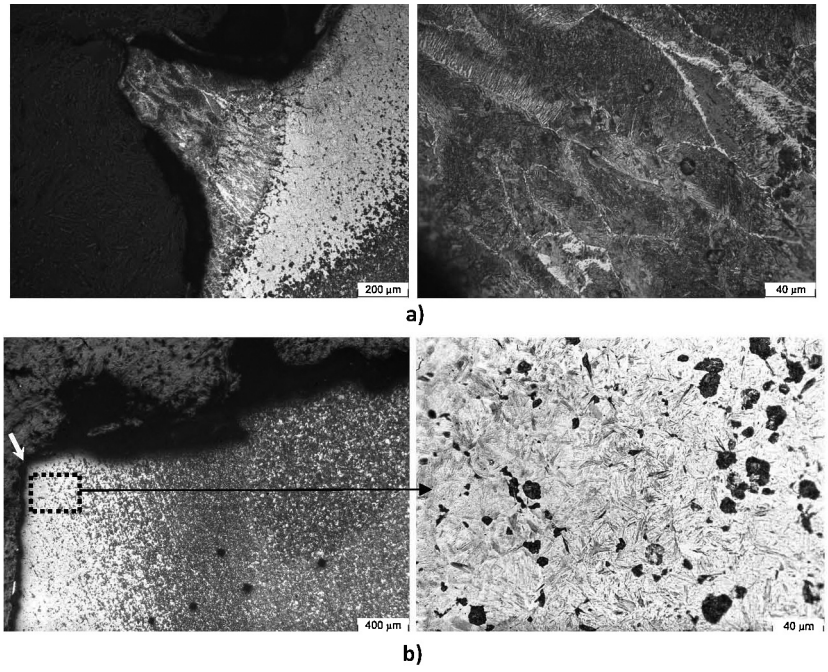

Fig. 5. AS-induced microstructure: (a) microstructure of the molten metal showing a columnar grain structure with proeutectoid ferrite and ferrite side plates at the prior austenitic grain boundaries and intracolumnar very fine perlite. (b) Under the molten metal: martensite with a significant profusion of defects in the prior austenitic grain boundaries; the white arrow indicates the fracture initiation point.

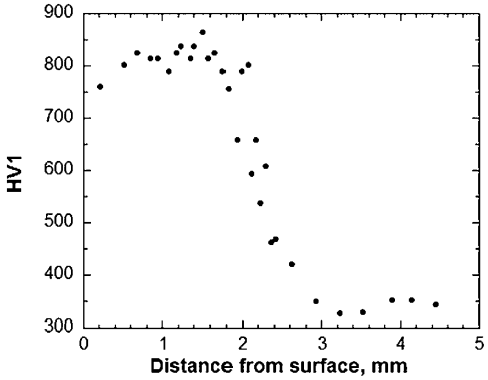

Fig. 6. Variation of the Vickers hardness (9.8 N) with distance from the bar surface in the AS affected zone.

the cracking runs parallel to the contour of the solidified molten metal (Fig. 7), the possible damage to the threadbar is limited to the AS-affected material spalling. These defects are similar to those referred to in welding as "cold cracking" [10].

It is known that for cold cracking to occur, three conditions must simultaneously be present. There must be a sufficient level of hydrogen; there must be a sensitive microstructure (martensite of a very high hardness); and there must be a sufficiently high level of constraint induced residual stress [10].

The hydrogen in molten metal results from the arc-induced dissociation of organic molecules on the bar surface or environmental moisture. Because the molten metal was not environmentally protected during the AS process, it is probable that hydrogen was present in the molten metal and martensitic layer. Furthermore, as shown in Fig. 5(a) (right), in the molten metal, the spherical cavities around the inclusions are presumably a consequence of the recombination of atomic hydrogen to form molecular hydrogen or even methane bubbles from the reaction of carbon with hydrogen. Because of the low martensite toughness, the hydrogen bubbles at the martensitic layer grow and merge to form extensive intergranular discontinuities, as shown in Fig. 5(b) (right).

The microstructure sensitivity level depends on the cooling rate from high temperatures and on the chemical composition of the material. A very high cooling rate (martensitic microstructure of very high hardness) and a constraint level (high residual stresses) are expected because of the local nature of AS. Regarding the chemical composition, it is well known that if the carbon equivalent (C_{eq}) is less than 0.4, the material is insensitive to cracking, and if it is larger than 0.6, the material is very sensitive to cracking [10]. In the present case, the C_{eq} is 0.82.

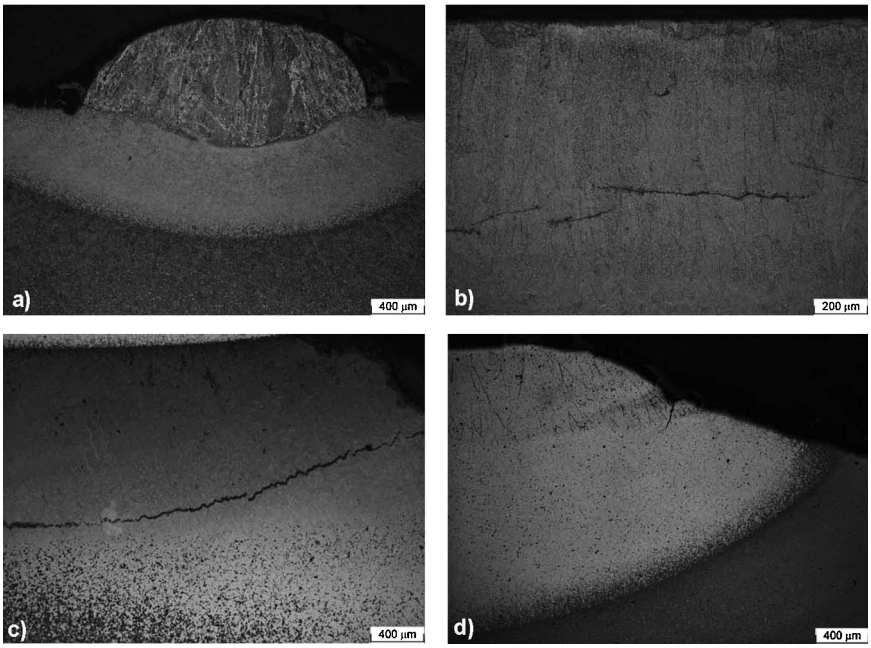

Fig. 7. Optical micrographs showing the representative details found in the bars of the AS-induced damage. (a) No macroscopic AS-induced damage. (b) Crack at the molten metal parallel to the bar axis. (c) Crack at the heat affected zone bordering the molten metal. (d) Surface crack at the toe of the molten metal.

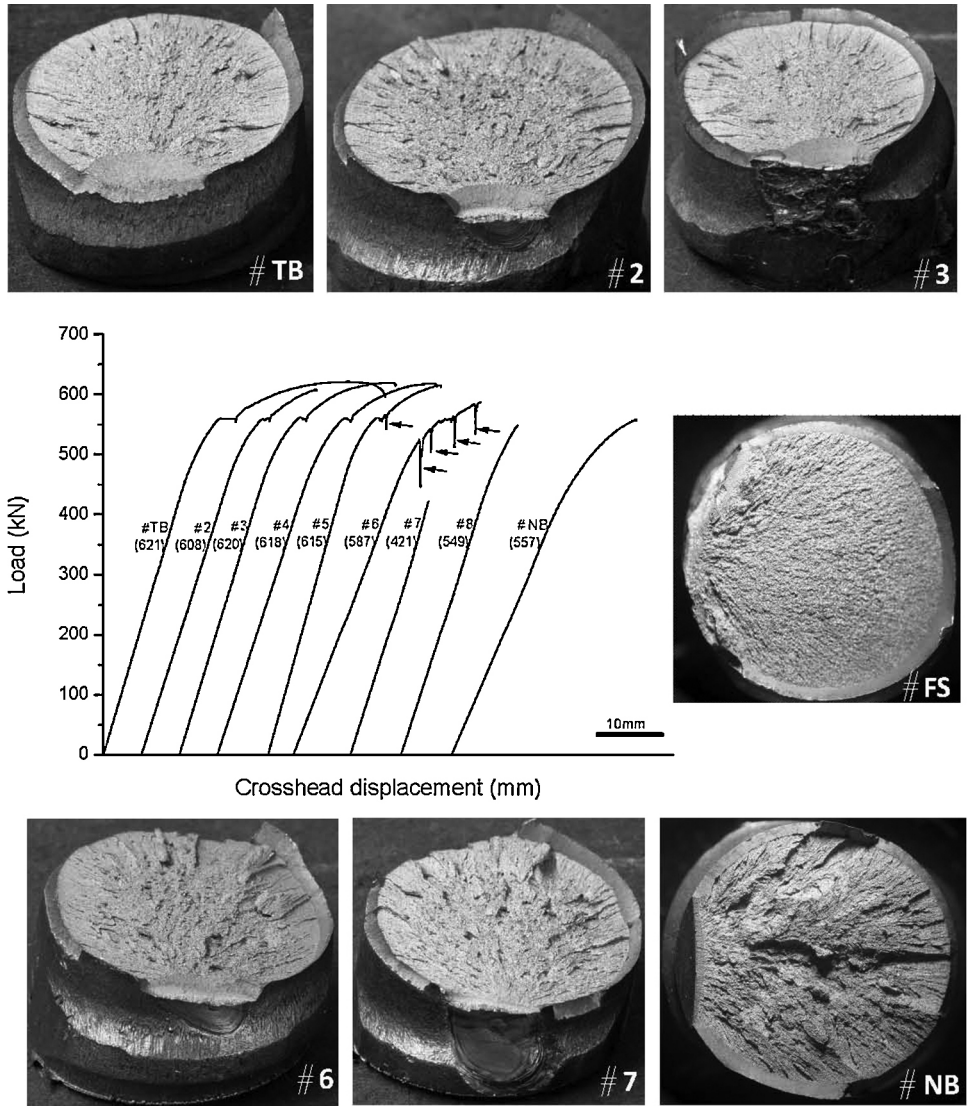

Fig. 8. Load-displacement curves for the undamaged (test #TB), AS-affected (tests #2 to #8), and notched (test #NB) bars, and macrofractographs showing the appearance of the fracture surface of the samples. Additionally, for comparative purposes, the fracture appearance of the broken during service threadbar is shown. The black arrows indicate a pop in. The numbers in brackets are the rupture load values.

Therefore, it is concluded that the threadbar material is very sensitive to cold cracking when AS occurs.

Tensile samples of the AS-affected threadbar were tested at the same conditions as the abovementioned undamaged sample. Fig. 8 shows the AS effect on the tensile behavior and the corresponding fracture appearance. For comparative purposes, the following information was included in the figure: the test curve of an undamaged threadbar (TB), the test curve of a threadbar with a transverse arc-shaped notch with a 100 mm curvature radius, 0.25 mm thickness and 1.95 mm depth (NB); and the fracture appearance of the bar that was broken during service (FS). The first conclusion one draws from this figure is the wide tensile behavior variation of the AS-affected threadbar. It is remarkable that for some samples (#2, #3, #4, and #5) the AS did not affect the yield load. Whereas for others (#3 and #4), the AS did not affect the yield load or the ultimate load. However, the location of the rupture is AS-determined. In test #5, a local brittle fracture (pop-in) was noted during tensile testing, but the material fracture toughness was sufficient to stop the crack and allow further plastic deformation to reach the final brittle fracture condition. In test #6, four pop-ins took place prior to reaching the final brittle fracture condition. Test #7 was the only test in which the sample broke in the elastic region of the load-elongation curve prior to reaching the service load of 0.7 times the ultimate load. Moreover, the fractographic features of the fracture surface of the sample are very similar to that of the fractured bar in service. It is worth mentioning that except for test #7, in the remaining tests, some ductile crack extension prior to the final brittle fracture was produced. In tests #8 and #NB, the final brittle fracture took place at approximately the yield load. It is clear that the AS-induced defect severity can be higher than in the notched sample.

3.1. Fractographic analysis

Fig. 4(a) (bottom) shows the macroscopic view of the fracture in service. The fracture surface immersion in a 6 N hydrochloric acid solution containing 2 g/L of hexamethylenetetramine inhibitor for 1 min was sufficient to gently remove the traces of rust from the fracture surface.

Fig. 9 shows a series of SEM micrographs taken at different positions along the fracture surface near the fracture initiation point. SEM micrographs #1 and #2 show the fractographic features of the spalled zone. SEM micrograph #1 of the molten metal fracture surface shows a mixture with a similar ratio of microvoid coalescence and intergranular brittle fracture. SEM micrograph #2 shows the fracture surface morphological features of the unmelted heat affected zone that consists of the intergranular brittle fracture and, to a lesser extent, microvoid coalescence. The fractographic features near the fracture initiation point (SEM micrograph #3) consisted of the cleaved facets with some microvoid coalescence zones. When the region near the initiation site was studied at successively higher magnifications, it was not possible to identify the microstructural feature that triggered fracture initiation from the converging segment of distinct fan-like radiating fracture patterns. The fractographic features in SEM micrographs #4 and #5, which correspond to the crack propagation stage, primarily consist of the cleavage facets with isolated patches of microvoid coalescence.

Although the failure mechanism of the threadbar it is still not fully clear, the above findings seem to indicate that a microcrack initiates at the martensitic layer and propagates unsteadily toward the bar surface across the molten metal to form a semielliptical surface crack. If crack extends throughout the remainder bar cross section depend on the size of that surface crack. If the crack size is smaller than a critical value a pop in will take place, as occurred in the tests #5 and #6 (Fig. 8). Otherwise, the dynamically growing crack will extend across the remainder cross section.

4. Mechanical analysis

There are two experimental results which enable that the linear elastic fracture mechanics is the appropriate tool to perform mechanical analysis of the threadbar failure. First, because of the brittle aspect of the fracture surfaces of both the threadbar broke in service and that corresponding to the sample of test #7 (Fig. 8) are nearly identical. Second, because of the

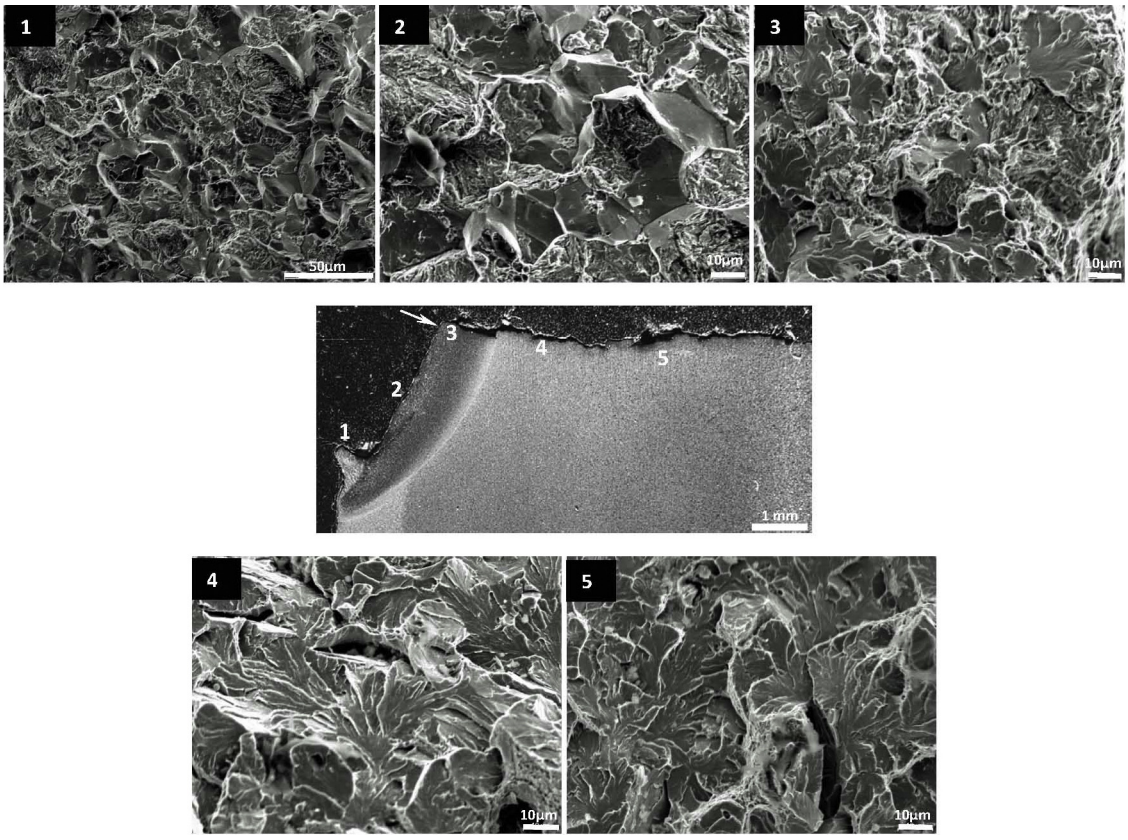

Fig. 9. SEM fractographs of the bar broken during service. The #1 and #2 SEM fractographs show the intergranular brittle fracture with microvoid coalescence at the spalled zone. The #3 SEM fractographs show the cleavage fracture with isolated areas of microvoid coalescence near the initiation point. The #4 and #5 SEM fractographs show the essentially brittle fracture with extensive cleavage facets at the unsteady propagation zone. The white arrow indicates the fracture initiation point.

load-elongation curve of the test #7 revealed that the rupture took place in the elastic region of the curve. From the broken bar analysis, it is understood that the fracture was triggered by a semielliptical crack with semi-major and semi-minor axes of 4.5 mm and 2.5 mm lengths, respectively. The stress intensity factor for a cylindrical bar with a semielliptical surface crack was calculated using the following expression [11]:

$$K_I = \frac{4P}{\pi D^2}\sqrt{\pi a}\sum\sum C_{ij}\left(\frac{a}{D}\right)^i\left(\frac{a}{b}\right)^j \quad (2)$$

where P is the applied load, D is the bar diameter, C_{ij} are the interpolation coefficients (given in Table 2 of Ref. [11]), and a and b are the lengths of the semi-minor and semi-major axes.

Because the linear elastic fracture mechanics is applicable, the fracture load is obtained using the following fracture criterion:

$$K_I - K_{Ic} \quad (3)$$

Considering the following data: $D = 26.5$ mm; $a = 2.5$ mm; $b = 4.5$ mm and $K_{Ic} = 70$ MPa m$^{1/2}$, the calculated fracture load was 467 kN, which is slightly higher than the design load of 435 kN. This load shows a good correlation with the design load, considering any experimental scatter and the fact that the calculated is only 7% higher than the design load. However, there are two factors which could cause further reduction in the service load of a threaded bar with an AS. First, the fracture toughness value to be considered is not that of the massive material but that of the heat affected material ahead the current crack tip. Second, due to the dynamic character of the initiation of the AS inducted fracture, the bar failure is not controlled by the static fracture toughness (K_{Ic}) but the crack-arrest toughness (K_{Ia}) which is significantly lower [12].

5. Recommendations

In terms of the equivalent carbon, the steel used for the manufacture of prestressed threadbars is not weldable. Therefore, it should be neither welded nor locally heated to high temperatures.

Contact with molten slag and unintentional arcing should be anticipated.

The work system should include protection and inspection of the bars until the completion of any welding work.

Acknowledgements

The authors thank L.D. Real of CENIM for his technical help with the generation of arc strikes.

References

[1] Valiente A, Elices M. Premature failure of prestressed steel bars. Eng Fail Anal 1998;5:219–27.
[2] Elices M, Valiente A, Caballero L, Iordachescu M, Fullea J, Sánchez-Montero J, et al. Failure of prestressed anchor bars. Eng Fail Anal 2012;24:57–66.
[3] ISO 15630-3:2010 Steel for the reinforcement and prestressing of concrete – test methods. Part 3. Prestressing steel.
[4] ISO 6892-1:2009 Metallic materials – tensile testing. Part 1. Method of test at room temperature.
[5] ASTM A722/A 722M:2003 Standard specification for uncoated high-strength steel bars for prestressing concrete.
[6] ASTM E1820:2013 Standard test method for measurement of fracture toughness.
[7] Structural welding code. Steel. ANSI/AWS D1.1-96. 15th ed. Florida: American Welding Society; 1996. 172, 402.
[8] Weisman , editor. 7th ed., Welding handbook. Fundamentals of welding, vol. 1, 7th ed. Florida: American Welding Society; 1976. p. 212.
[9] Boling B. Understanding arc strikes. Insp Trends 2013;16(3):22–5.
[10] Easterling K. Introduction to the physical metallurgy of welding. London: Butterworths; 1983. p. 180–94.
[11] Astiz MA. An incompatible singular elastic element for two and three dimensional crack problems. Int J Fract 1986;31:105–23.
[12] Nakano Y, Tanaka M. Crack arrest toughness of structural steels evaluated by compact test, Trans ISIJ, 22, 147–153.